

Comprehensive Analysis for Shifting MIMO SAR System

Sang Ho Lim*

Abstract—Synthetic aperture radar (SAR) system has inherent constraints between high azimuth resolution and wide swath width. Achieving more phase center samples is one of the key solutions to resolve this limitation. By multiple N transmitting and N receiving channel concept, an increased resolution or a widened swath width could be obtained. In this paper, comprehensive analysis for shifting multiple-input multiple-output (MIMO) SAR system is presented. System resolution enhancement has been demonstrated based on the distributed target simulation by a factor of N compared to conventional displaced phase center antenna (DPCA) system.

1. INTRODUCTION

Conventional synthetic aperture radar (SAR) systems which use a single antenna aperture for transmitting (Tx) and receiving (Rx), have inherent limit for achieving a wide swath width W_g and a good azimuth resolution ρ_a together. This limitation can be expressed about pulse repetition frequency (PRF) as follows:

$$\frac{v_p}{\rho_a} \approx \Delta f_d < \text{PRF} < \frac{c}{2 \cdot W_g \cdot \sin(\theta_i)} \quad (1)$$

where v_p is airborne or spaceborne platform velocity, Δf_d the Doppler bandwidth, c the speed of light and θ_i the incident angle. From this inequity, PRF boundary could be determined with considering an appropriate azimuth resolution and a suitable swath width.

Airborne SAR system has a large boundary about the PRF because of the slower velocity and smaller swath width than spaceborne SAR system. For those reasons, a high PRF for obtaining both wide swath width and high resolution can be simply selected [1]. For spaceborne SAR system, which has a faster platform velocity and a wider required swath width, several novel studies based on the displaced phase center antenna (DPCA) technique have been introduced for overcoming the constrains [2–6].

Using the conventional DPCA system, we can obtain additional samples in the azimuth direction by a factor of N, which is the number of Rx channels, during each pulse repetition interval (PRI). By increasing the number of samples, an improved azimuth resolution or a decreased PRF can be achieved by a factor of N. When considering the Tx and Rx channels for the systems, DPCA SAR system can be explained as a single-input multiple-output (SIMO) system. For getting more samples, novel multiple-input multiple-output (MIMO) SAR system concept design based on a multiple Tx antenna shift method has been introduced [7], and various types of MIMO SAR systems have received much attention due to their attractive application potentials [10–13]. The shifting MIMO SAR system has N^2 samples during one PRI, and it results in an increased azimuth resolution or the decreased operating PRF by a factor of N, number of Tx channels, compared to the DPCA-based SAR systems.

In this paper, comprehensive analysis for the proposed shifting MIMO SAR system is presented. Figure 1 shows the total block diagram of the suggested shifting MIMO SAR system which includes a Tx pulse generation set, an air interface, Rx demodulation, dividers, range compression, phase

Received 4 January 2016, Accepted 4 March 2016, Scheduled 20 March 2016

* Corresponding author: Sang Ho Lim (limsangho@kaist.ac.kr).

The author is with the Department of Electrical Engineering, Korea Advanced Institute of Science and Technology (KAIST), 291 Daehak-ro, Yuseong-Gu, Daejeon 305-701, Republic of Korea.

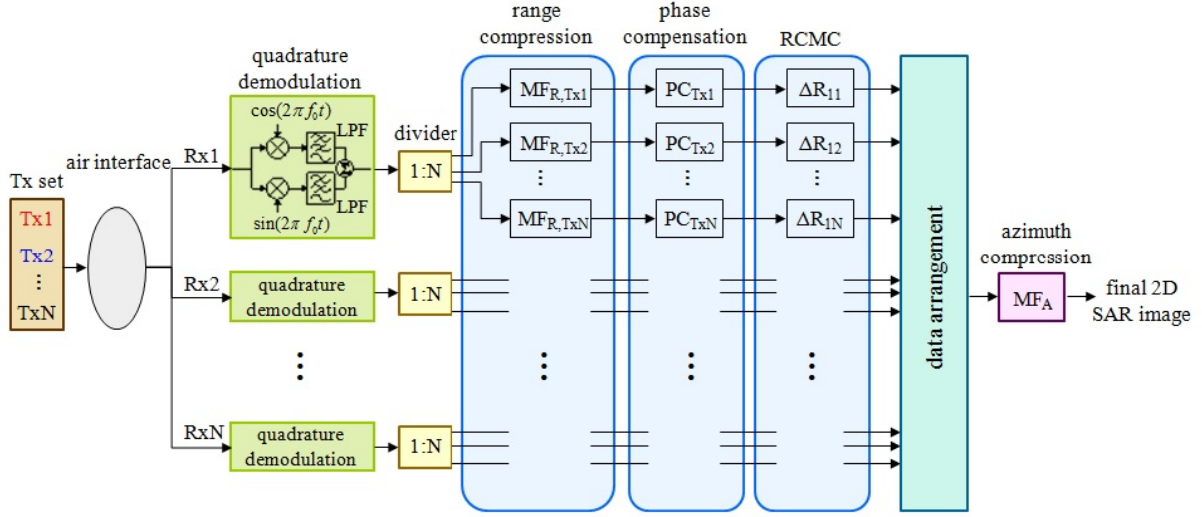


Figure 1. Total block diagram of proposed shifting MIMO SAR system.

compensation, range cell migration correction (RCMC), data arrangement, and azimuth compression blocks. Through the phase compensation blocks, we can consider the phase errors caused by the discrete distribution of element antennas of a large array. Based on the detailed total system analysis, it would be straightforwardly possible to apply this suggested method to real spaceborne SAR system. This paper is organized as follows. In Section 2, I briefly explain the suggested shifting MIMO SAR system compared to the conventional DPCA-based SAR system. In Section 3, a detailed analytical description of the proposed shifting MIMO SAR system is presented. The performance analysis based on a distributed target simulation is presented in Section 4. I conclude the paper with a brief summary in Section 5.

2. SHIFTING MIMO SAR SYSTEM AND CONSTRAINTS

Figure 2 shows a comparison between a DPCA-based SAR system, which has a single fixed Tx and three Rx antennas, and the suggested shifting MIMO SAR system with three Tx and Rx antennas. The timing diagrams of both systems are illustrated in Figure 2(a). In contrast to the DPCA-based SAR system, a Tx set which has multiple Tx pulses is used for the suggested system. Each Tx pulse is emitted at each shifted Tx antenna with a pulse duration τ and pulse interval $\Delta\tau$.

As we can observe in Figure 2(b), the number of sample positions in one PRI in the DPCA-based SAR system is equal to that of the receiving channels, 3; on the other hand, the shifting MIMO SAR system can obtain 3^2 sample positions in the same PRI with the help of shifting strategy.

To obtain the same distance between samples, the movement of the platform during the previous pulse transmissions has to be considered. If not, the delayed samples are obtained and cause significant error as shown in Figure 3.

The platform movement for the previous pulse transmission can be represented as follows:

$$\Delta m_i = (i - 1) \cdot (\tau_i + \Delta\tau) \cdot v_p \quad (2)$$

where Δm_i is the distance of the movement of the platform when the i -th pulse is emitted. In order to compensate the movement of the platform, the space desired to be shifted for the Tx antenna at each pulse can be derived as follows:

$$\Delta s_i = \frac{(i - 1) \cdot \Delta x}{N} - 2 \cdot \Delta m_i \quad (3)$$

where Δs_i is the shifted space of the i -th Tx antenna, and the first term of this equation represents the space for the stop and hop case, and the second term explains the compensation of the platform movement. After applying the equation, identical distance between samples can be obtained as shown in Figure 4.

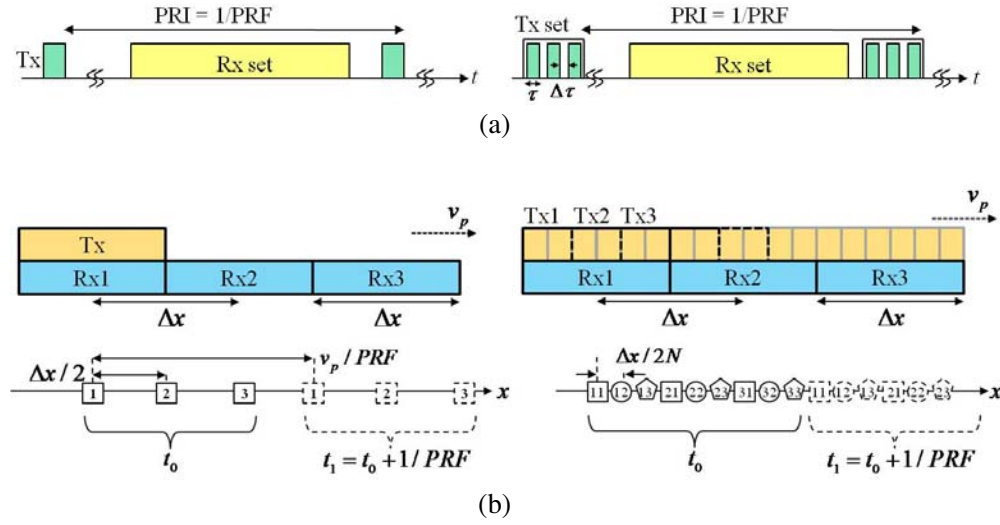


Figure 2. Comparison between a DPCA-based SAR and proposed shifting MIMO SAR. (a) Timing diagrams of DPCA-based SAR (left) and proposed shifting MIMO SAR (right). (b) Spatial sampling points of DPCA-based SAR (left) and proposed shifting MIMO SAR (right).

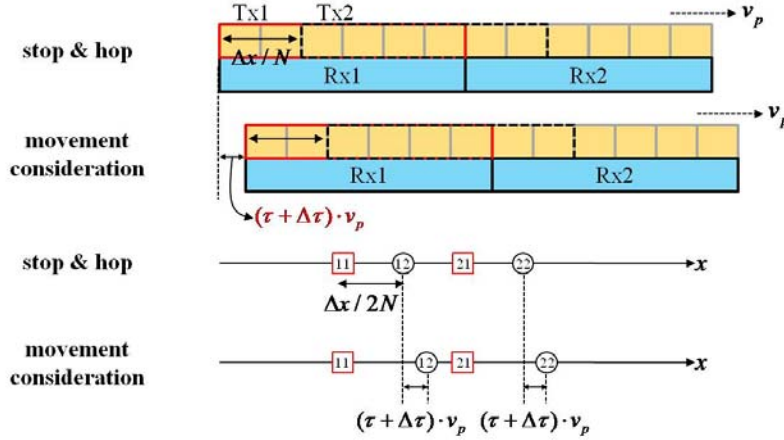


Figure 3. Necessity of a platform movement consideration.

The shifted space Δs_i should be greater than or equal to zero to guarantee the system operation. Therefore, the maximum number of Tx and Rx antennas of the shifting MIMO SAR system can be derived as following equations.

$$\Delta s_i \geq 0 \quad (4)$$

$$N \leq \frac{\Delta x}{2 \cdot (\tau_i + \Delta\tau) \cdot v_p} \quad (5)$$

Another important issue when designing the shifting MIMO SAR system is the Tx antenna shift error because of the discrete distribution of element antennas of a large array antenna. So the shifted space Δs_i given from Eq. (3) cannot be adjusted arbitrarily in a real array antenna system.

Figure 5 shows the antenna geometry in azimuth direction. The desired shifted space, Δs_i , can be represented by the sum of the real shifted space, Δs_i^r , and the space to be compensated, Δs_i^c , as shown

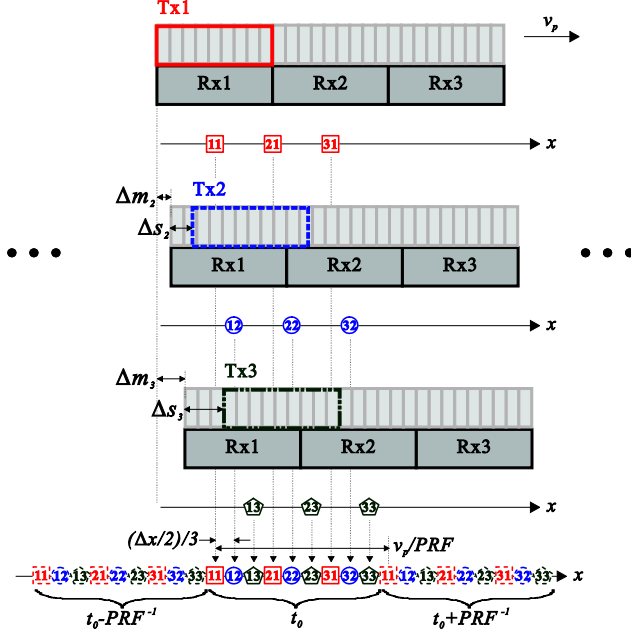


Figure 4. Spatial sampling positions after applying the platform movement effect.

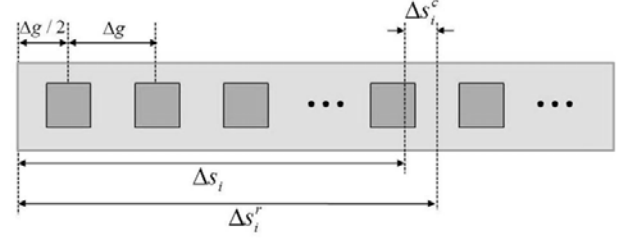


Figure 5. Antenna geometry in azimuth direction.

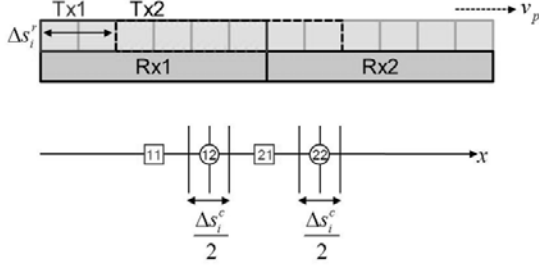


Figure 6. Phase center position change.

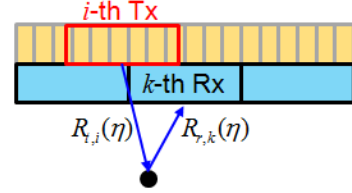


Figure 7. The instant slant ranges between the target and the phase centers of the i -th Tx antenna and the k -th Rx antenna, respectively.

in Eq. (6).

$$\Delta s_i = \text{round} \left(\frac{\Delta s_i}{\Delta g} \right) \cdot \Delta g + \text{frac} \left(\frac{\Delta s_i}{\Delta g} \right) = \Delta s_i^r + \Delta s_i^c \quad (6)$$

$$-\frac{\Delta g}{2} \leq \Delta s_i^c \leq \frac{\Delta g}{2} \quad (7)$$

where Δg is the gap between the element antennas. Since the phase center positions are placed at the middle point between the Tx antenna and Rx antenna, the phase center position change due to the Tx antenna shift error is half of the space to be compensated as shown in Figure 6.

$$-0.175\lambda \leq \frac{\Delta s_i^c}{2} \leq 0.175\lambda \quad (8)$$

If we assume that the gap equals 0.7λ , the range of error can be represented as Eq. (8), and it is quite small compared to the distance between the phase centers. So we do not need to change the antenna beam pattern in order to compensate the error. However, the phase variation needs to be considered and is compensated in phase compensation stage which will be explained in next section.

3. COMPREHENSIVE ANALYSIS FOR PROPOSED SYSTEM

In this section, a more detailed analytical description of the shifting MIMO SAR system is given. The whole block diagram of the suggested shifting MIMO SAR system is expressed in Figure 1. Tx pulses with slope-varying chirp signals can be used to achieve low cross-correlation [8]. The i -th Tx signal can be expressed as follows:

$$s_{tx,i}(t) = A_i \cdot w_{r,i}(t) \cdot \cos(2\pi f_0 t + \pi K_{r,i} t^2) \quad (9)$$

$$w_{r,i}(t) = \text{rect}\left(\frac{t}{\tau_i}\right) \quad (10)$$

where f_0 is the operating frequency, and A_i , $w_{r,i}(t)$, $K_{r,i}$, and τ_i are the amplitude, range window function, range linear frequency modulation (LFM) rate, and pulse duration of the i -th Tx signal, respectively. $\text{rect}(x)$ is the rectangular function defined by

$$\text{rect}(x) = \begin{cases} 1, & \text{if } |x| \leq 0.5 \\ 0, & \text{otherwise} \end{cases} \quad (11)$$

The Tx pulse set $s_{tx}(t)$ can be expressed with the time delay of each pulse as in Eq. (9), below.

$$s_{tx}(t) = \sum_{i=1}^N s_{tx,i} \left[t - \left(\frac{\Delta m_i}{v_p} \right) \right] \quad (12)$$

The total Tx pulses are emitted and then reflected from a ground through the air interface. Each receiver is turned on to obtain the reflected signals, and the signal arrived at the k -th Rx antenna can be represented as follows:

$$s_{rx,k}(t, \eta) = \sum_{i=1}^N B_{ki} \cdot w_a(\eta) \cdot s_{tx,i} \left[t - \left(\frac{\Delta m_i}{v_p} \right) - \frac{R_{t,i}(\eta) + R_{r,k}(\eta)}{c} \right] \quad (13)$$

where

$$R(\eta) = \sqrt{R_0^2 + v_p^2 \eta^2} \approx R_0 + \frac{v_p^2 \eta^2}{2R_0} \quad (14)$$

$$R_{t,i}(\eta) = R \left[\eta - \left(\frac{\Delta s_i^r}{v_p} \right) \right] \quad (15)$$

$$R_{r,k}(\eta) = R \left[\eta - \frac{(k-1) \cdot \Delta x}{v_p} \right] \quad (16)$$

$$R_{t,1}(\eta) = R_{r,1}(\eta) = R(\eta) \quad (17)$$

η is the azimuth time; B_{ki} is the complex radar cross section (RCS); $w_a(\eta)$ is the azimuth beam pattern that can be extended using the method [1]; $R_{t,i}(\eta)$ and $R_{r,k}(\eta)$ are the instant slant ranges between the target and the phase centers of the i -th Tx antenna and the k -th Rx antenna, respectively as shown in Figure 7; $R(\eta)$ is the standard slant range which is the distance between the target and the phase center of the first Tx antenna; R_0 is the slant range of closet approach.

Substituting Eq. (9) into Eq. (13) gives

$$\begin{aligned} s_{rx,k}(t, \eta) = & \sum_{i=1}^N B_{ki} \cdot w_a(\eta) \cdot A_i w_{r,i} \left[t - \left(\frac{\Delta m_i}{v_p} \right) - \frac{R_{ki}(\eta)}{c} \right] \\ & \cdot \cos \left\{ 2\pi f_0 \left[t - \left(\frac{\Delta m_i}{v_p} \right) - \frac{R_{ki}(\eta)}{c} \right] + \pi K_{r,i} \left[t - \left(\frac{\Delta m_i}{v_p} \right) - \frac{R_{ki}(\eta)}{c} \right]^2 \right\} \end{aligned} \quad (18)$$

where

$$R_{ki}(\eta) = R_{t,i}(\eta) + R_{r,k}(\eta) \quad (19)$$

The received signal is down-converted using the quadrature demodulation, and the k -th baseband signal can be expressed as follows:

$$\begin{aligned}
 s_{rxk}(t, \eta) = & \sum_{i=1}^N B_{ki} \cdot A_i w_{r,i} \left[t - \left(\frac{\Delta m_i}{v_p} \right) - \frac{R_{ki}(\eta)}{c} \right] \cdot w_a(\eta) \\
 & \cdot \exp \left[-j2\pi f_0 \left(\frac{\Delta m_i}{v_p} \right) \right] \cdot \exp \left(-j \frac{4\pi}{\lambda_0} R_0 \right) \\
 & \cdot \exp \left[j \frac{-\pi (\Delta s_{ki}^-)^2}{2\lambda_0 R_0} \right] \cdot \exp \left\{ -j\pi K_a \left[\eta - \left(\frac{\Delta s_{ki}^+}{2v_p} \right) \right]^2 \right\} \\
 & \cdot \exp \left\{ j\pi K_{r,i} \left[t - \left(\frac{\Delta m_i}{v_p} \right) - \frac{R_{ki}(\eta)}{c} \right]^2 \right\}
 \end{aligned} \tag{20}$$

where

$$K_a = 2v_p^2 / (\lambda_0 R_0) \tag{21}$$

$$\Delta s_{ki}^- = \Delta s_i^r - (k-1) \cdot \Delta x \tag{22}$$

$$\Delta s_{ki}^+ = \Delta s_i^r + (k-1) \cdot \Delta x \tag{23}$$

The exponential terms of Eq. (20) express phase variations due to Tx pulse delay, slant range R_0 , different azimuth displacements between Tx and Rx antennas, azimuth and range modulations. Each baseband signal is now equally divided into N paths and compressed in the range direction by independently using N matched filter. The range compressed signal of the k -th Rx antenna with l -th Tx matched filter as in Eq. (24) can be represented using the principle of stationary phase (POSP) [9] as in Eq. (25).

$$h_{r,l}(t, \eta) = \exp(-j\pi K_{r,l} t^2) \tag{24}$$

$$\begin{aligned}
 s_{rc}^{kl}(t, \eta) = & \frac{1}{N} \left\{ B_{kl} A_l \cdot p_r^l \left[t - \left(\frac{\Delta m_l}{v_p} \right) - \frac{R_{kl}(\eta)}{c} \right] \cdot AP_{kl}(\eta) \right\} \\
 & + \frac{1}{N} \sum_{\substack{i=1 \\ i \neq l}}^N B_{ki} A_i \cdot q_r^{il} \left[t - \left(\frac{\Delta m_i}{v_p} \right) - \frac{R_{ki}(\eta)}{c} \right] \cdot AP_{ki}(\eta)
 \end{aligned} \tag{25}$$

where

$$p_r^l(t) = \frac{\exp(\text{sgn}_l \cdot j\pi/4)}{\sqrt{|K_{r,l}|}} |K_{r,l}| \tau_l \cdot \text{sinc}(|K_{r,l}| \tau_l t) \tag{26}$$

$$\begin{aligned}
 q_r^{il} = & \sqrt{\frac{|K_{r,l}|}{|K_{r,i} - K_{r,l}|}} \cdot \exp \left[\frac{(\text{sgn}_i + \text{sgn}_{il}) \cdot j\pi}{4} \right] \\
 & \cdot \text{rect} \left(\frac{|K_{r,l}| t}{|K_{r,i} - K_{r,l}| \tau_i} \right) \cdot \exp \left\{ \left[\frac{-j\pi \cdot K_{r,i} K_{r,l}}{(K_{r,i} - K_{r,l}) \tau_i} \right] t^2 \right\}
 \end{aligned} \tag{27}$$

$$\text{sgn}_l = \begin{cases} 1, & K_{r,l} > 0 \\ -1, & K_{r,l} < 0 \end{cases} \tag{28}$$

$$\text{sgn}_{il} = \begin{cases} 1, & \frac{K_{r,i} - K_{r,l}}{K_{r,i} K_{r,l}} > 0 \\ -1, & \frac{K_{r,i} - K_{r,l}}{K_{r,i} K_{r,l}} < 0 \end{cases} \tag{29}$$

$$\begin{aligned}
 AP_{ki}(\eta) = & w_a(\eta) \cdot \exp \left[-j2\pi f_0 \left(\frac{\Delta m_i}{v_p} \right) \right] \cdot \exp \left(-j \frac{4\pi}{\lambda_0} R_0 \right) \\
 & \cdot \exp \left[j \frac{-\pi (\Delta s_{ki}^-)^2}{2\lambda_0 R_0} \right] \cdot \exp \left\{ -j\pi K_a \left[\eta - \left(\frac{\Delta s_{ki}^+}{2v_p} \right) \right]^2 \right\}
 \end{aligned} \tag{30}$$

The first part of Eq. (25) is the autocorrelation, and the second part represents the cross-correlations. The power difference level between them can be expressed in log scale as follows:

$$20 \cdot \log_{10} \left(\sqrt{|K_{r,i} - K_{r,l}|} \cdot \tau_i \right) \quad (31)$$

We can select the range LFM rates and pulse durations to make power difference level less than -30 dB. From this process, we can omit the term related with cross-correlations in Eq. (25) and obtain N^2 independent signals after applying range compression using N matched filters.

To correctly recover the N^2 compressed signals, the phase variations due to the Tx pulse delay of Eq. (2) and different azimuth displacements between the Tx and Rx antennas of the third exponential term in Eq. (20) have to be compensated by adding the following term:

$$PC_{ki} = \exp \left[j2\pi \left(\frac{\Delta m_i}{v_p} f_0 + \frac{(\Delta s_{ki}^-)^2}{4\lambda_0 R_0} \right) \right] \quad (32)$$

In order to compensate the Tx antenna shift error mentioned in the previous section, I added the following term in the range Doppler domain.

$$PC_{ki}(f_\eta) = \exp \left[\left(\frac{j2\pi}{v_p} \Delta s_i^c \right) f_\eta \right] \quad (33)$$

The phase compensated signal can be expressed in the range Doppler domain as follows:

$$S_{pc}^{kl}(t, f_\eta) = \frac{B_{kl} A_l}{N} \cdot p_r^l \left[t - \left(\frac{\Delta m_l}{v_p} \right) - \frac{R_{kl}(f_\eta)}{c} \right] \cdot AP_{kl}^{pc}(f_\eta) \quad (34)$$

where

$$R_{kl}(f_\eta) = 2R_0 + \frac{v_p^2}{R_0} \left[\left(\frac{f_\eta}{K_a} + \frac{\Delta s_{kl}^+}{2v_p} \right)^2 + \frac{(\Delta s_{kl}^-)^2}{4v_p^2} \right] \quad (35)$$

$$AP_{kl}^{pc}(f_\eta) = W_a(f_\eta) \cdot \exp \left(-j \frac{4\pi}{\lambda_0} R_0 \right) \cdot \exp \left(\frac{j\pi}{K_a} f_\eta^2 \right) \cdot \exp \left\{ \frac{j2\pi}{v_p} \left[\frac{-((k-1)N + l - 1) \cdot \Delta x}{2N} + \Delta m_l \right] f_\eta \right\} \quad (36)$$

f_η is the azimuth frequency and $W_a(f_\eta)$ the envelope of Doppler spectrum of the antenna azimuth beam pattern. The position of the phase center between the l -th Tx antenna and k -th Rx antenna is given in the first term in the square brackets in Eq. (36). The second term demonstrates the compensation for the movement of the platform when the l -th pulse is emitted.

The total phase centers from the suggested MIMO SAR system have N^2 positions in one PRI as shown in Eq. (37), below. Each row is obtained from the corresponding Rx antenna, and each column is related with the corresponding Tx antenna.

$$-\frac{\Delta x}{2N} \begin{bmatrix} 0 & \dots & l-1 & \dots & N-1 \\ \vdots & \ddots & \vdots & \ddots & \vdots \\ (k-1)N & \dots & (k-1)N + l - 1 & \dots & kN - 1 \\ \vdots & \ddots & \vdots & \ddots & \vdots \\ (N-1)N & \dots & (N-1)N + l - 1 & \dots & N^2 - 1 \end{bmatrix} \quad (37)$$

N^2 phase compensated signals move to the next step of the RCMC, and the quantity to be corrected is as follows:

$$RCM_{kl}(f_\eta) = - \left(\frac{\Delta m_l \cdot c}{v_p} \right) - \frac{v_p^2}{R_0} \left[\left(\frac{f_\eta}{K_a} + \frac{\Delta s_{kl}^+}{2v_p} \right)^2 + \frac{(\Delta s_{kl}^-)^2}{4v_p^2} \right] \quad (38)$$

After applying the RCMC, the corrected signal can be expressed as follows:

$$S_{rcmc}^{kl}(t, f_\eta) = \frac{B_{kl} A_l}{N} \cdot p_r^l \left[t - \frac{2R_0}{c} \right] \cdot AP_{kl}^{pc}(f_\eta) \quad (39)$$

N^2 corrected signals, as arranged in Equation (40), below, fill in the gaps of the target's azimuth phase history.

$$S_{da}(t, f_\eta) = \begin{bmatrix} S_{\text{rcmc}}^{11}(t, f_\eta) \\ S_{\text{rcmc}}^{12}(t, f_\eta) \\ \vdots \\ S_{\text{rcmc}}^{1N}(t, f_\eta) \\ \vdots \\ S_{\text{rcmc}}^{N1}(t, f_\eta) \\ S_{\text{rcmc}}^{N2}(t, f_\eta) \\ \vdots \\ S_{\text{rcmc}}^{NN}(t, f_\eta) \end{bmatrix} \quad (40)$$

$$H_a(f_\eta) = \exp \left[-j\pi f_\eta^2 / (K_a) \right] \quad (41)$$

After applying the azimuth matched filter in Eq. (41) to the data set of Eq. (40), we can, finally, obtain a 2-dimensional SAR image in the range Doppler domain as Eq. (42) and the range azimuth time domain as Eq. (43) when normalization criteria is used.

$$S_{ac}(t, f_\eta) = \text{sinc} \left[|K_{r,1}| \tau_1 \left(t - \frac{2R_0}{c} \right) \right] \cdot W_a(f_\eta) \cdot \exp \left(-j \frac{4\pi}{\lambda_0} R_0 \right) \quad (42)$$

$$s_{ac}(t, \eta) = \text{sinc} \left[|K_{r,1}| \tau_1 \left(t - \frac{2R_0}{c} \right) \right] \cdot p_a(\eta) \cdot \exp \left(-j \frac{4\pi}{\lambda_0} R_0 \right) \quad (43)$$

where

$$|K_{r,1}| \tau_1 = |K_{r,2}| \tau_2 = \dots = |K_{r,N}| \tau_N \quad (44)$$

$p_a(\eta)$ is the amplitude of the azimuth impulse response based on the antenna azimuth beam pattern. Using the azimuth beam pattern extension [1] and the shifting MIMO SAR system concept, a high resolution image can be obtained without ambiguity.

Table 1. System parameters and simulation cases.

| General parameters | | | Value | | | |
|--------------------------|--------------------------|-----------|------------------|-----------|-----------|---------|
| Carrier frequency | | | 9.7 (GHz) | | | |
| Platform height | | | 580 (km) | | | |
| Platform velocity | | | 7560 (m/s) | | | |
| Chirp signal bandwidth | | | 300 (MHz) | | | |
| Interval between pulses | | | 5 (μ s) | | | |
| Incident angle | | | 20°–55° | | | |
| Element antenna (EA) gap | | | 0.7 λ_0 | | | |
| | DPCA-based SAR system | | | | | |
| | Δx (m) | No. of EA | Beam width (deg) | No. of Tx | No. of Rx | TAL (m) |
| Case 1 | 4 | 180 | 0.4 | 1 | 3 | 12 |
| Case 2 | 3 | 135 | 0.52 | 1 | 4 | 12 |
| | Proposed MIMO SAR system | | | | | |
| | Δx (m) | No. of EA | Beam width (deg) | No. of Tx | No. of Rx | TAL (m) |
| Case 3 | 4 | 180 | 1.2 | 3 | 3 | 12 |
| Case 4 | 3 | 135 | 2.1 | 4 | 4 | 12 |

· TAL: Total antenna length

4. PERFORMANCE ANALYSIS USING DISTRIBUTED TARGET

In order to generalize the proposed shifting MIMO SAR system, the distributed target simulations are carried out using the parameters summarized in Table 1. The beamwidth of each Tx and Rx antenna is extended by a factor of N following the method suggested in [1]. Figure 8 shows a comparison between antenna azimuth beam patterns for each case.

Figure 9 shows the map of KAIST in Dae-jeon in Korea, and some area is selected to be used for

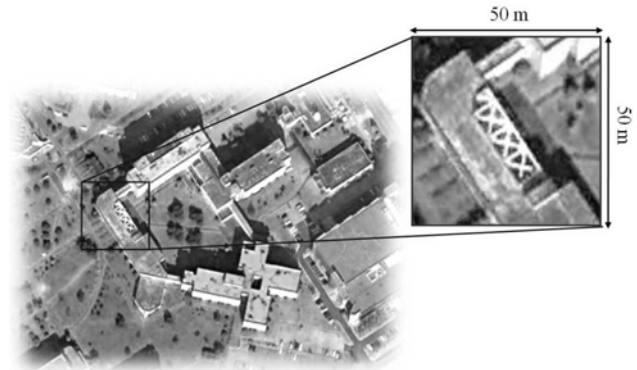
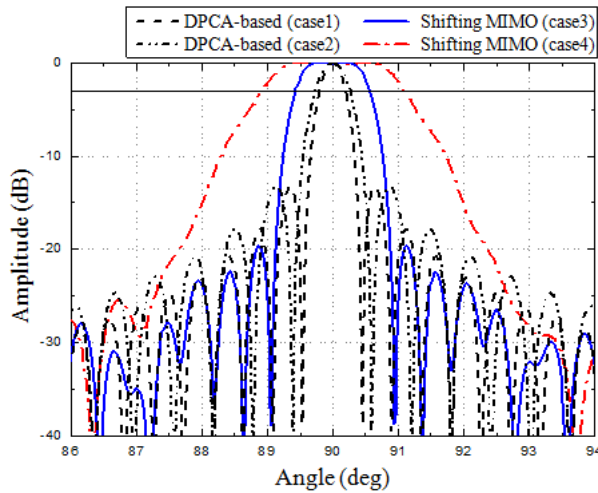


Figure 8. Antenna azimuth beam pattern comparison between DPCA-based SAR systems and proposed shifting MIMO SAR systems.

Figure 9. Original image for distributed target simulation.

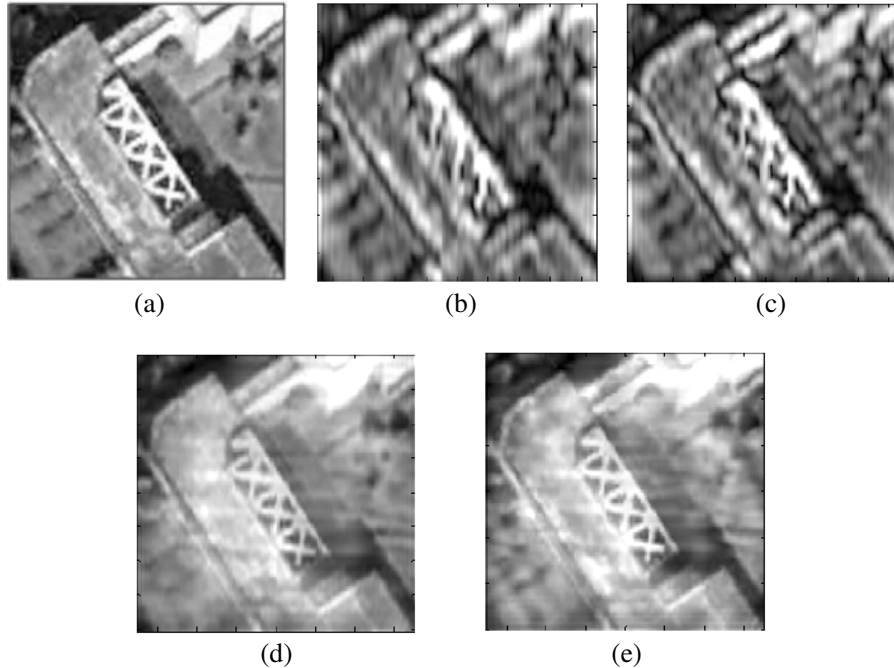


Figure 10. Comparison of the distributed target simulation results. (a) Original image. (b) DPCA (Case 1; resol.: 2.08 m). (c) DPCA (Case 2; resol.: 1.52 m). (d) Shifting MIMO (Case 3; resol.: 0.7 m). (e) Shifting MIMO (Case 4; resol.: 0.41 m).

Table 2. Azimuth resolution comparison.

| | DPCA-based SAR system | | Proposed shifting MIMO SAR system | |
|--------------|-----------------------|--------|-----------------------------------|--------|
| | Case 1 | Case 2 | Case 3 | Case 4 |
| ρ_a (m) | 2.08 | 1.52 | 0.70 | 0.41 |

simulation. The gray-scaled bitmap image can be considered as the reflectivity map of the area. Regions of zero RCS are indicated by black color, while regions of high RCS are indicated by white color. The minimum cell resolution of the area is $0.25 \cdot 0.25 \text{ m}^2$. Since the area of the chosen region is $50 \cdot 50 \text{ m}^2$, the number of total targets in the area is 40,000.

Figure 10 represents the results of the distributed target simulations for the DPCA-based SAR system and the proposed shifting MIMO SAR system. To mitigate the image distortion between range and azimuth directions, various chirp pulse bandwidths are used. As shown in this figure, the azimuth resolution of the shifting MIMO SAR system was improved by a factor of 3 for Case 3 and 4 for Case 4 as compared to the conventional DPCA-based SAR system, as summarized in Table 2.

5. CONCLUSION

In this paper, detailed analysis for a shifting MIMO SAR system has been introduced. From the Tx pulse generation blocks to azimuth compression blocks, we can see the radar signal's comprehensive logical expressions. Especially, during the phase compensation step, we can compensate the phase errors caused by the discrete distribution of element antennas of a large array. The shifting MIMO SAR system can obtain N^2 samples during one PRI, and it can result in increased azimuth resolution by a factor of N , the number of Tx channels, compared to the DPCA-based SAR system. This is confirmed by the distributed target simulations. Based on the suggested comprehensive analysis for this shifting MIMO SAR system, it can be possible to effectively enhance the system performance of future spaceborne SAR systems.

REFERENCES

1. Lim, S., J.-H. Han, S.-Y. Kim, and N.-H. Myung, "Azimuth beam pattern synthesis for airborne SAR system optimization," *Progress In Electromagnetics Research*, Vol. 106, 295–309, 2010.
2. Gebert, N. and G. Krieger, "Azimuth phase center adaptation on transmit for high-resolution wide-swath SAR imaging," *IEEE Geosci. Remote Sens. Lett.*, Vol. 6, 782–786, 2009.
3. Krieger, G., N. Gebert, and A. Moreira, "Unambiguous SAR signal reconstruction from nonuniform displaced phase center sampling," *IEEE Geosci. Remote Sens. Lett.*, Vol. 1, 260–264, 2004.
4. Suess, M., B. Grafmüller, and R. Zahn, "A novel high resolution, wide swath SAR system," *Proc. IGARSS*, 1013–1015, 2001.
5. Callaghan, G. D. and I. D. Longstaff, "Wide swath spaceborne SAR using a quad element array," *Proc. Inst. Elect. Eng. — Radar, Sonar, Navigat.*, Vol. 146, 159–165, 1999.
6. Currie, A. and M. A. Brown, "Wide-swath SAR," *Proc. Inst. Elect. Eng. — Radar, Sonar, Navigat.*, Vol. 139, 122–135, 1992.
7. Lim, S. H., C. G. Hwang, S. Y. Kim, and N. H. Myung, "Shifting MIMO SAR system for high-resolution wide-swath imaging," *Journal of Electromagnetic Waves and Applications*, Vol. 25, Nos. 8–9, 1168–1178, 2011.
8. Soumekh, M., "SAR-ECCM using phase-perturbed LFM chirp signals and DRFM repeat jammer penalization," *IEEE Trans. Aero. Elect. Sys.*, Vol. 42, 191–205, 2006.
9. Cumming, I. G. and F. H. Wong, *Digital Processing of Synthetic Aperture Radar Data, Algorithms and Implementation*, 625, Artech House, Boston, 2005.

10. Krieger, G., "MIMO-SAR: Opportunities and pitfalls," *IEEE Transactions on Geoscience and Remote Sensing*, Vol. 52, 2628–2645, 2014.
11. Hossain, M. A., A. Elshafiey, and M. A. S. Alkanhal, "High-resolution and wide-swath UWB OFDM MIMO synthetic aperture radar system using image fusion," *Journal of the Indian Society of Remote Sensing*, Vol. 43, 225–242, 2015.
12. Huang, Y., G. Liao, J. Xu, and D. Yang, "MIMO SAR OFDM chirp waveform design and GMTI with RPCA based method," *Digital Signal Processing*, Vol. 51, 184–195, 2016.
13. Wang, W. Q., "MIMO SAR OFDM chirp waveform diversity design with random matrix modulation," *IEEE Transactions on Geoscience and Remote Sensing*, Vol. 53, 1615–1625, 2015.